Conference on Modelling Fluid Flow (CMFF'22)
The 18th International Conference on Fluid Flow Technologies
Budapest, Hungary, August 30-September 2, 2022

Investigations on the Separation of Two Immiscible Liquids in Helical Pipes with Different Conditions and Dimensions

Michael MANSOUR[1,2], Conrad MÜLLER[3], Dominique THÉVENIN[4], Katharina ZÄHRINGER[5]

[1] Corresponding Author. Mechanical Power Engineering Department, Faculty of Engineering - Mataria, Helwan University, 11718 Cairo, Egypt. E-mail: m.botros@m-eng.helwan.edu.eg
[2] Lab. of Fluid Dynamics & Technical Flows, University of Magdeburg "Otto von Guericke", 39106 Magdeburg, Germany. Tel.: +493916758569, Fax: +493916742840, E-mail: michael.mansour@ovgu.de
[3] Lab. of Fluid Dynamics & Technical Flows, University of Magdeburg "Otto von Guericke", 39106 Magdeburg, Germany. E-mail: conrad.mueller@ovgu.de
[4] Lab. of Fluid Dynamics & Technical Flows, University of Magdeburg "Otto von Guericke", 39106 Magdeburg, Germany. E-mail: thevenin@ovgu.de
[5] Lab. of Fluid Dynamics & Technical Flows, University of Magdeburg "Otto von Guericke", 39106 Magdeburg, Germany. E-mail: katharina.zaehringer@ovgu.de

ABSTRACT

The separation of two immiscible liquids in helical pipes was investigated in this study. Assuming perfectly mixed liquids at the pipe inlet, the flow conditions and pipe dimensions have been varied in order to study the separation performance. The two immiscible liquids are water and amine. Three different pipe orientations were compared, i.e., vertical upward, vertical downward, and horizontal flow. A laminar flow is considered, covering the optimal range of Reynolds numbers (around Re = 225-563) for separation. Additionally, the separation behaviour was compared in two different pipe diameters. The Volume Of Fluid (VOF) method was used to model the contact surface between the two immiscible liquids. The separation is quantified using the average mixing coefficient of the two liquids. Companion experiments to validate the results of this numerical study are currently running.

Keywords: CFD, Effect of geometrical parameters, Helical pipes, Immiscible liquids, Liquid-liquid separation and mixing, VOF

NOMENCLATURE

A	$[m^2]$	cross-sectional area
A_f	$[m^2]$	grid face area
D	$[m]$	coil diameter
L	$[m]$	length of coil
M_c	$[-]$	mixing coefficient
P	$[m]$	coil pitch
V	$[m^3]$	volume of computational cell
V_m	$[m^3]$	volume of phase m
X/L	$[-]$	dimensionless axial length
CFL	$[-]$	Courant–Friedrichs–Lewy number
De	$[-]$	Dean number
Re	$[-]$	superficial Reynolds number
d	$[m]$	pipe diameter
f_b	$[N]$	body force
g	$[m/s^2]$	gravitational acceleration
i	$[-]$	unit vector of Cartesian axes
k	$[-]$	number of fluid phases
n	$[-]$	number of turns
p	$[N/m^2]$	pressure
u	$[m/s]$	flow velocity
v	$[m/s]$	average flow velocity
$\overline{V}$	$[m^3]$	Average volume of computational cell
α	$[-]$	volume fraction
α_m	$[-]$	local grid volume fraction of phase m
δ	$[-]$	curvature ratio (d/D)
γ	$[-]$	dimensionless pitch $(P/\pi D)$
μ	$[Pa\ s]$	dynamic viscosity
$\overline{\alpha_\mathrm{m}}$	$[-]$	surface-averaged volume fraction of phase m
ρ	$[kg/m^3]$	density

Subscripts and Superscripts

a, m, w	amine, phase m, water
f	grid face
c	coefficient

1. INTRODUCTION

In helical pipes, a centrifugal force is generated due to the fluid motion in a curved path, creating a secondary flow in the form of counter-rotating vortices (also known as Dean vortices) even for laminar flow conditions [1]. Due to this secondary flow, the performance of helical pipes concerning several processes like mixing, heat transfer, mass transfer, and residence time distributions is improved when compared to that of straight pipes [2–6]. Helical pipes provide other advantages when used for such processes as they involve no moving parts, need no source of power, and are compact in design. Accordingly, helical pipes need low maintenance and consume low energy. On the other hand, the pressure drop in helical pipes is usually higher compared to a straight pipe of the same length [4].

Multiphase flows of immiscible fluids can be found in important physical and chemical applications, comprising petroleum, food, oil, nuclear, polymer, and pharmaceutical industries [5]. The flow of immiscible fluids can involve gas-liquid or liquid-liquid flows. The complexity of such flows depends strongly on the properties of the phases, their volume fractions, and the flow regime (e.g., disperse, slug, plug, segregated...). Furthermore, the presence of the centrifugal force and the secondary flow in helical pipes add to the complexity when investigating such flows [5].

Numerous studies can be found in the literature for the flow in helical pipes concerning miscible fluids [3, 4, 6–9] as well as immiscible fluids [5, 10–13]. When investigating miscible fluids in helical pipes, researchers consider mainly the overall flow features, the structure of the generated vortices, mixing performance, enhancement of heat/mass transfer, and process intensification in general.

Similarly, different objectives are considered for studies examining immiscible fluids in helical pipes (as in the present work). For instance, the enhancement of mass transfer between two immiscible liquids in a curved pipe was investigated by Gelfgat et al. 2003 [11]. Their results showed that the intensity of Dean vortices does not increase in a monotonous manner when increasing Reynolds number (Re). They found an optimal value of Reynolds number at Re = 50 to enhance mass transfer for the considered pipe dimensions.

The phase distributions and the flow regimes of immiscible liquid-liquid flows in helical and curved pipes were thoroughly studied in the literature. Three main flow regimes were found in the study of Sharma et al. 2011 [14] for a kerosene–water flow through curved return bends, including stratified, plug, and dispersed flow regimes. Though they found no significant effect of the flow orientation (upward, downward, or horizontal) on the flow regimes, this may be due to the small pipe length considered in their study (only a half-coil turn). In the experimental studies of Pietrzak 2014 [15] as well as Ali and Mandal 2019 [10] for oil-water two-phase flows, additional flow regimes were observed, such as dispersed (drops), plugs, stratified, wavy, and annular-dispersed flows. These flow regimes were found different when compared to those of straight pipes, whereas it was shown that the viscosity plays a key role concerning flow regimes [10]. Based on pipe dimension and flow conditions, numerous flow regimes can be obtained for curved pipes, as found in some recent studies [16].

Several applications necessitate separation of fluid phases, including for instance pharmaceutical and oil industries [17], to extract, isolate, purify, re-use, or recover either of the phases. However, the separation of immiscible fluids is not easy once the fluids are in contact. Examples of known separation techniques are distillation [18], chromatography [19], filtration [20], centrifugation [21], and gravity settling [22]. These techniques depend on various forces like centrifugal, buoyant, surface tension, capillary, viscous, and/or gravitational force, as well as combinations of them to separate the phases [23]. Consequently, numerous types of separators can be found in the literature. However, most separators are complex in design, limited to specific applications, or not suited for continuous processes.

The simple and compact design of helical pipes was considered for separation processes in several studies. For instance, Zhang et al. 2006 [12] investigated the separation of oil-water flows in a coiled configuration. It was shown that the separation is normally faster when the water droplet diameter is larger. It was also found that the increase of the flow rate or the reduction of the curvature ratio can improve the separation [12, 24]. However, this is valid only for a restricted flow range due to the continuous change of vortical structure with the flow rate [3, 4, 25, 26]. This was confirmed in gas-liquid separation studies in a helical configuration, where it was revealed that the trend of the separation behaviour changes for different flow rates [13, 23]. For example, three different trends were found in [13] by increasing the fluid velocity, i.e., increasing, decreasing, and increasing again. A similar conclusion was reported in [23], where the increase of the centrifugal force was not always positive concerning separation. This is mainly happening because the flow velocity affects the structure of the Dean vortices, the magnitude of different forces acting on the flow, and the residence time available for separation. Accordingly, there exist optimal conditions (in particular in terms of the Reynolds number) for fluid separation in helical pipes.

Based on the literature, the underlying process is still not fully understood. Additionally, most of the previous studies involve some limitations, i.e., too short pipes, a single pipe orientation, a single measurement location (outlet), and/or a limited range of flow conditions. Therefore, the present work investigates in more detail the separation behaviour, particularly when the fluids are initially perfectly mixed at the inlet, which is common in industrial processes. For example, to improve chemical reactions, catalysts should be highly dispersed and well mixed with the main flow. In our previous study [27], the flow of two immiscible liquids (amine and water) in helical and straight pipes was studied computationally to identify optimal separation conditions. It was shown that the separation is very limited in straight pipes for different orientations, while a very good separation was obtained in a horizontal helical pipe at an optimal water Reynolds number of about 225. However, a single helical pipe with constant dimensions was considered. Accordingly, in the present paper, we extend these investigations further by considering helical pipes with two different pipe diameters. An implicit, unsteady, and segregated solver was employed. The Volume Of Fluid (VOF) method was used to model the interface between the two immiscible liquids. The separation was quantified using the average mixing coefficient of the two liquids [3, 4]. Companion experiments to validate the results of this numerical study are currently running.

2. NUMERICAL MODELING

2.1. Governing equations

For transient conditions, Cartesian coordinates, an incompressible, Newtonian, and adiabatic flow, the governing equations of the CFD (Computational Fluid Dynamics) model can be written as: Continuity equation:

$$\frac{\partial u_i}{\partial x_i} = 0, \tag{1}$$

Momentum equation:

$$\rho\left(\frac{\partial u_i}{\partial t} + u_j\frac{\partial u_i}{\partial x_j}\right) = -\frac{\partial p}{\partial x_i} + \frac{\partial}{\partial x_j}\left[\mu\left(\frac{\partial u_i}{\partial x_j} + \frac{\partial u_j}{\partial x_i}\right)\right] + \rho g_i + f_\mathrm{b}, \tag{2}$$

where $i = 1, 2, 3$, p is the pressure, u is the velocity, μ is the dynamic viscosity, ρ is the density, g is the gravitational acceleration, and f_b is the body force.

2.2. Volume Of Fluid method

The Volume Of Fluid method (VOF) was used to model the interactions between the two immiscible fluids. The VOF technique was initially established to predict the interface between different fluids. In the VOF formulation, an additional transport equation is solved for the local volume fraction (α) of the liquids, while keeping the benefit of modeling the two fluids by one set of conservation equations (one-fluid formulation). Common velocity, pressure, and temperature fields are assumed. The VOF method was successfully employed in several studies considering immiscible fluids, showing reliable results, e.g., [27–31]. In a flow of k phases (here, k = 2), the phase volume fraction of phase m is given by:

$$\alpha_\mathrm{m} = \frac{V_\mathrm{m}}{V} \tag{3}$$

where, V_m is the volume of the phase m in the computational cell, and V is the volume of the cell. In each cell, the summation of the volume fractions of all phases must be one. Accordingly, based on the volume fraction, the existence of different fluids in a computational cell can be distinguished. If a phase m is not existing in a cell, a value of $\alpha_\mathrm{m} = 0$ is expected, while $\alpha_\mathrm{m} = 1$ means that the phase m completely fills the cell. The phase volume fraction between 0 and 1 ($0 < \alpha_\mathrm{m} < 1$) indicates partial presence of the phase m, which also means that the cell contains a local interface between both phases. The scalar transport equation of the volume fraction of phase m (α_m) is given by:

$$\frac{\partial \alpha_\mathrm{m}}{\partial t} + \vec{u} \cdot \frac{\partial \alpha_\mathrm{m}}{\partial x_i} = 0 \tag{4}$$

For the cells containing a local interface, the mixture properties are determined based on the fraction of each phase.

2.3. Mixing and separation quantification

The mixing coefficient (M_c) was used to quantify the separation behaviour in the present work [3,4,27, 28]. The mixing coefficient indicates how well the phases are mixed (or separated) on a specific cross-section. It can be calculated for a phase m over a cross-sectional area of A by:

$$M_{\mathrm{c\ m}} = 1 - \frac{\sum_\mathrm{f} |\alpha_\mathrm{m} - \overline{\alpha_\mathrm{m}}| A_\mathrm{f}}{|\overline{\alpha_\mathrm{m}}| \sum_\mathrm{f} A_\mathrm{f}} \tag{5}$$

with

$$\overline{\alpha_\mathrm{m}} = \frac{1}{A}\int \alpha_\mathrm{m}\, dA \tag{6}$$

where $\overline{\alpha_\mathrm{m}}$ is the surface-averaged volume fraction of phase m over the cross-sectional area A, and A_f is the area of a computational cell face. To obtain the overall mixing value M_c of the two liquids, the mixing coefficient is calculated individually for each liquid, and then an average is calculated. Note that, the separation would be easier if the liquids are only incompletely mixed [12]. Accordingly, a value of M_c = 1 means 100% mixing (i.e., no separation at all), which was assumed always at the inlet, representing the worst-case initial condition for the separation of the liquids.

2.4. Numerical settings

The CFD code STAR-CCM+ was employed to perform the numerical simulations. An implicit, unsteady, and segregated solver was used. The second-order upwind scheme was chosen for calculating the convective fluxes. Further, the first-order upwind scheme was set for temporal discretization. To ensure that the maximum local Courant–Friedrichs–Lewy number (CFL) is always lower than 1, an adaptive time step was utilized, where the CFL number was calculated based on the maximum velocity and the minimum cell size of the whole domain. Accordingly, the time step varies in the approximate range between 2×10^{-4} and 8×10^{-4} s. Ten inner iterations were necessary to ensure convergence of all absolute residuals within each time step. The simulations were stopped after a total physical time of at least 1.4 times the average residence time of the flow in the pipes. For instance, the total physical time computed was 20 and 75 s for the superficial Reynolds number of water $\mathrm{Re_w}$ = 563 and $\mathrm{Re_w}$ = 225,

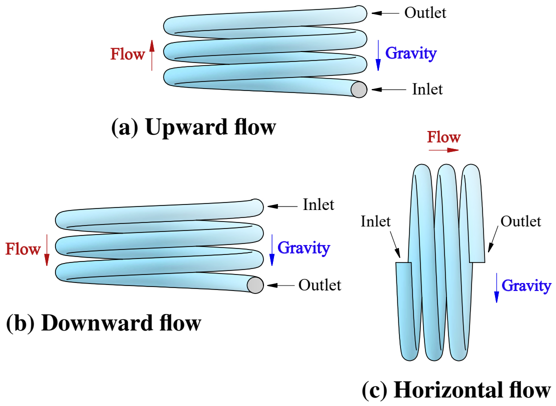

Figure 1. Different orientations considered.

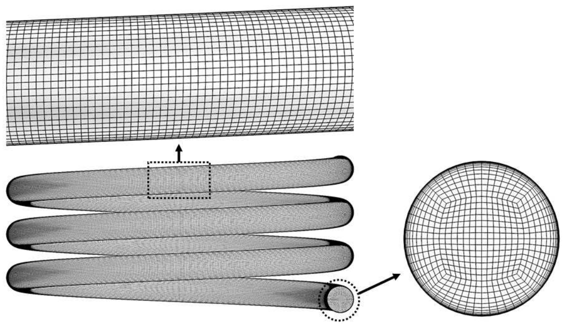

Figure 2. Sample view of the applied hexahedral mesh (G1 with 1.85 million cells).

respectively. A no-slip boundary condition was set on the walls. At the inlet of the computational domain, a Hagen-Poiseuille parabolic velocity profile was considered, to avoid the numerical errors coming with the plug-flow (uniform velocity) assumption [3]. Additionally, a perfect mixture was always set at the inlet surface (100% mixing, $M_c = 1$) with a volume fraction of 0.5 for each liquid. This condition corresponds to the theoretical worst case for the separation of the liquids. At the outlet surface, a constant-pressure boundary condition was applied.

2.5. Geometrical settings

As mentioned in the introduction, three different pipe orientations were considered in the investigations: horizontal, vertical upward, and vertical downward, as shown in Figure 1. The dimensions of the basic helical pipe (G1) were selected based on an existing prototype, which was used in several previous experimental and numerical studies [2–4,6,7,26,27]. The geometrical parameters of the different pipes considered in the present study are listed in Table 1. The first geometry (G1) has a pipe diameter of $d = 10$ mm, a coil diameter of $D = 118$ mm, a pitch of $P = 16$ mm, a total number of turns of $n = 3$, and total length of $L = n\sqrt{(\pi D)^2 + P^2} = 1112$ mm. G2 has similar dimensions except that the pipe diameter is $d = 5$ mm.

Table 1. Geometrical parameters of the different helical pipes considered in this study.

Coil	P mm	d mm	D mm	L mm	$\delta = d/D$	$\gamma = P/\pi D$	n
G1	16	10	118	1112	0.084	0.043	3
G2	16	5	118	1112	0.042	0.043	3

2.6. Flow conditions

The liquids considered are water and amine, typically found in the hydroformylation process [27]. The density of water is $\rho_w = 999.79$ kg/m^3, the density of amine is $\rho_a = 791$ kg/m^3, the dynamic viscosity of water is $\mu_w = 8.887 \cdot 10^{-4}$ Pa·s, the dynamic viscosity of amine, $\mu_a = 1.99 \cdot 10^{-3}$ Pa·s. The considered surface tension coefficient between water and amine is set to 0.0285 N/m [27]. Two different Reynolds numbers were studied as given in Table 2, corresponding to the optimal range for separation [27]. Re_w and Re_a are the superficial Reynolds numbers of water and amine, as defined by Equations 7 and 8, respectively, and v is the average velocity of the flow at the inlet surface. At the end, three flow cases with three different values of Dean number ($De = Re\sqrt{\delta}$) are considered as listed in Table 2.

$$Re_w = \frac{\rho_w v d}{\mu_w} \tag{7}$$

$$Re_a = \frac{\rho_a v d}{\mu_a} \tag{8}$$

Table 2. Different flow conditions considered.

Case #	Coil	v (m/s)	Re_a	Re_w	De_a	De_w
1	G1	0.02	79	225	23	65
2	G1	0.05	199	563	58	164
3	G2	0.04	79	225	16	46

3. COMPUTATIONAL MESH

The meshing parameters were selected based on previous studies after performing a mesh-independence test to ensure that mesh-independent results are obtained [27, 32]. Since the coil geometries have different dimensions, scale factors were used to always generate cell elements of the same size as in [27, 32], ensuring a constant resolution in space for all geometries. This leads to hexahedral grids with approximately 1.85 million cells for G1, while G2 has approximately 0.84 million cells. A sample view of a selected mesh is shown in Figure 2.

4. RESULTS AND DISCUSSIONS

4.1. Time averaging

For a specific cross-section, the instantaneous mixing coefficient M_c varies strongly with time due to the various flow regimes generated along the coil. Accordingly, a time-averaged value of M_c was used. When averaging on time intervals lower than 3 s, noticeable variations in the mixing coefficient values are observed; while, when averaging for more than 3.5 s, a stable average could be obtained. For in-

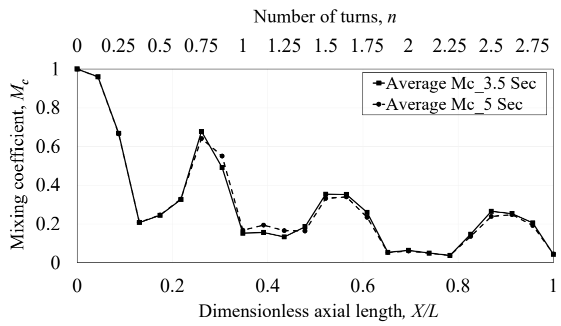

Figure 3. Time-averaged M_c of two different averaging times (3.5 or 5 s) for horizontal flow in G1 at Re_w = 563.

stance, the value of M_c obtained when averaging during 3.5 and 5 s are identical for the horizontal flow in G1 at Re_w = 563. The averaged M_c is shown in Figure 3 against the coil axial length. No significant changes can be seen between the averaged curves of the two time periods, confirming proper time averaging. Accordingly, a time duration of 3.5 s has been kept to calculate the time-averaged mixing coefficient.

4.2. Effect of pipe orientation

Figures 4a, 4b, 4c show the volume fraction of amine for upward, downward, and horizontal flow, respectively, at Re_w = 563 in G1. To track phase separation, the amine phase is represented in Figure 4 by (red) iso-surfaces that show all cells with amine volume fractions between 0.99 and 1 (almost pure amine). The blue color indicates almost pure water, while the green color represents a perfect mixture of the two liquids, as prescribed at the inlet surface.

For the upward flow shown in Figure 4a, a thin water layer separates and accumulates gradually on the lower side of the pipe due to its higher density. However, no significant separation is observed for this pipe orientation. This is also the case for the downward flow shown in Figure 4b, which shows only a minor separation of amine after two coil turns. On the other hand, rapid separation of amine is taking place after only half a turn as demonstrated in Figure 4c for the horizontal pipe orientation. Additionally, the amine phase is accumulating (red color) at the end of each turn, showing significant separation. Note that, the buoyant force changes direction each half-turn, allowing a local accumulation of amine (the lighter phase) before the maximum pressure (at the lowest part of each turn).

Figure 5 shows the minimum, average, and maximum mixing coefficients for different pipe orientations at Re_w = 563 in G1. For the upward flow shown in Figure 5a, the mixing coefficient drops progressively with the accumulation of water phase shown above, yet a very limited separation takes place. Similarly, a poor separation is taking place for the downward flow as shown in Figure 5b. Additionally, large fluctuations of the mixing coefficient occur in

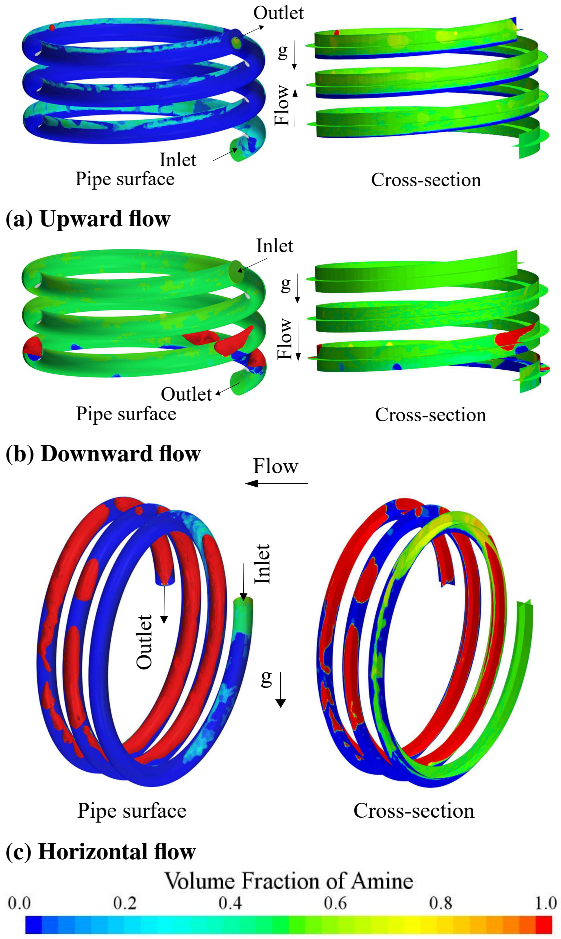

Figure 4. Upward, downward, and horizontal flow in G1 at Re_w =563.

the third coil turn due to the separation of amine droplets and slugs. For the horizontal flow, the average mixing coefficient fluctuates periodically along the pipe length corresponding to local accumulations of amine. Here, the average mixing coefficient is very low (0.04) after about two turns, with very limited changes between minimum, average, and maximum mixing coefficients, demonstrating very good separation.

4.3. Effect of Reynolds number

Figure 6 compares the volume fraction of amine (red represents pure amine) in G1 between Re_w = 225 and Re_w = 563. As shown, a very good separation takes place for both values. Nonetheless, a plug flow regime occurs on the left side of the pipe at Re_w = 225, while an intermittent flow regime is observed at Re_w = 563 on the same side. For the higher value of the Reynolds number, the residence time is lower, leading to a slightly lower separation (smaller accumulation of amine). The corresponding mixing coefficients are shown in Figure 7. Again, the mixing coefficient behaviour is similar for both Reynolds number values. However, it is slightly higher for Re_w = 563, due to the lower residence time.

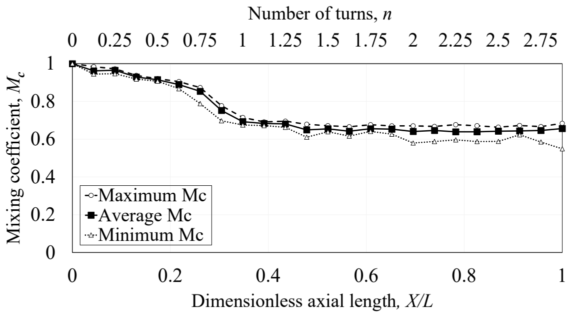

(a) Upward flow

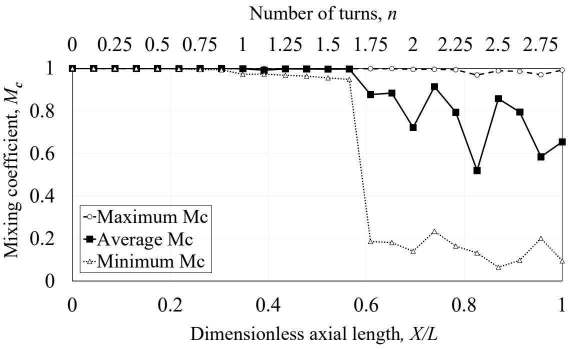

(b) Downward flow

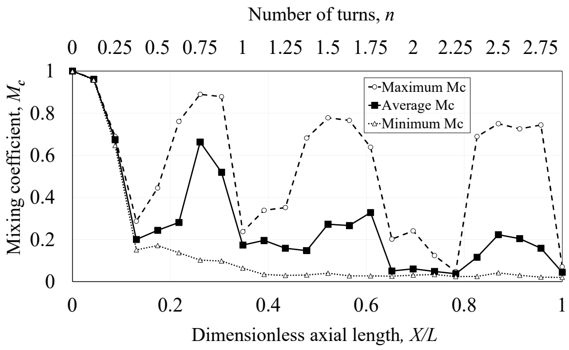

(c) Horizontal flow

Figure 5. Mixing coefficients in G1 at Re_w = 563.

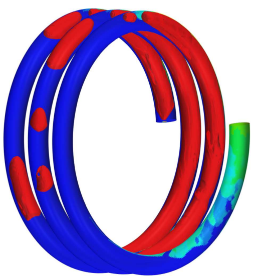

(a) Re_w = 225

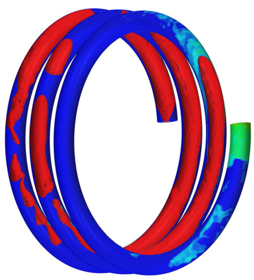

(b) Re_w = 563

Volume Fraction of Amine

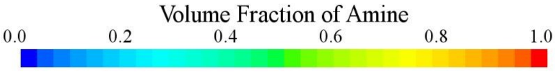

Figure 6. Volume fraction of amine for horizontal flow in G1 at Re_w = 225 and Re_w = 563.

4.4. Effect of pipe diameter

In this section, the influence of varying the pipe diameter is considered comparing G1 with d = 10

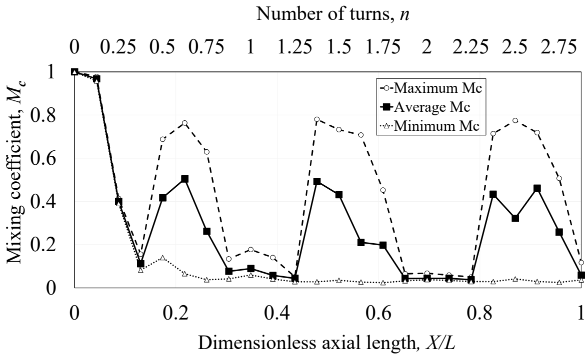

(a) Re_w = 225

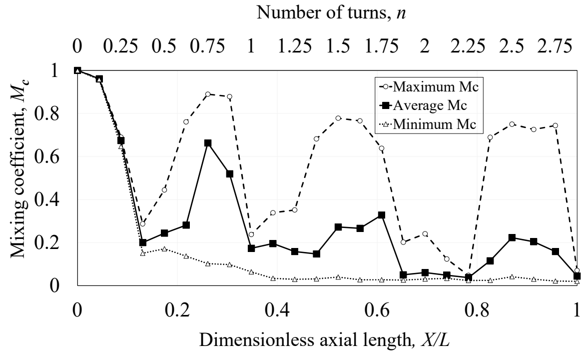

(b) Re_w = 563

Figure 7. Mixing coefficients for horizontal flow in G1 at Re_w = 225 and Re_w = 563.

mm and G2 with d = 5 mm for the same Reynolds number (Re_w=225); yet the Dean number is different due to the change in the curvature ratio (see again Tables 1 and 2). As shown in Figure 8, the separation is strongly reduced in the lower pipe diameter coil (G2), where a flow regime transition occurs and only a plug flow is observed after approximately two coil turns, leading to a very slow and improper separation. In G2, no accumulation of amine can be observed. This happens mainly due to the increased flow velocity and the strongly reduced residence time as well as the decreased curvature ratio. For the very low curvature ratios, the flow behaviour becomes close to that in a straight pipe, decreasing the separation. This reduced separation is quantified by the mixing coefficients as shown in Figure 9, where the values are much higher when compared to those of G1 shown in Figure 7a. Consequently, it would be recommended to utilize the horizontal orientation with appropriate flow conditions and pipe diameter to ensure efficient separation of immiscible liquids. The investigations will be extended in the future to study the other geometrical parameters as well as fluid properties.

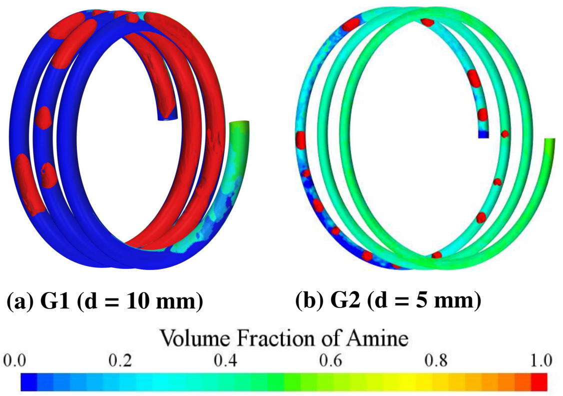

(a) G1 (d = 10 mm) **(b) G2 (d = 5 mm)**

Figure 8. Volume fraction of amine for horizontal flow in G1 and G2 at Re_w = 225.

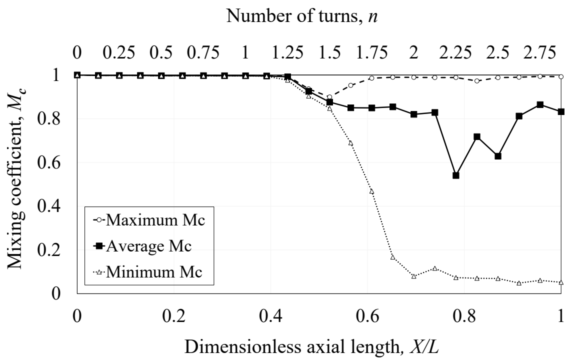

Figure 9. Mixing coefficients for horizontal flow in G2 at Re_w = 225.

5. CONCLUSION

The separation of two immiscible liquids (water and amine) in helical pipes was studied for various conditions. The Volume Of Fluid (VOF) method was used to model the contact surface between the two immiscible liquids. The separation is quantified using the average mixing coefficient of the two liquids. A perfect mixture was assumed at the pipe inlet, representing the worst case for the two liquids two separate. The separation performance was compared for three different pipe orientations, i.e., vertical upward, vertical downward, and horizontal flow. Additionally, two values of Reynolds number and pipe diameters were studied. Only very poor separation is happening in the upward and the downward flow, while the horizontal pipe orientation leads to much better separation. When increasing the Reynolds number from 225 to 563, the residence time decreases, leading to a slightly lower separation. Further, when reducing the pipe diameter from 10 to 5 mm at the same Reynolds number (225), a flow transition occurs, leading to a plug flow in the pipe, which eliminates the accumulation of the lighter phase and reduces the phase separation strongly. Accordingly, it would be generally recommended to employ the horizontal orientation with appropriate flow conditions and coil dimensions to ensure efficient separation of immiscible liquids.

ACKNOWLEDGEMENTS

The authors would like to thank the Deutsche Forschungsgemeinschaft (DFG, German Research Foundation) - TRR 63 “Integrated Chemical Processes in Liquid Multiphase Systems” (subproject B1) - 56091768 (Gefördert durch die Deutsche Forschungsgemeinschaft (DFG) - TRR 63 “Integrierte chemische Prozesse in flüssigen Mehrphasensystemen” (Teilprojekt B1) – 56091768).

REFERENCES

[1] Dean, W. R., 1927, “Note on the motion of fluid in a curved pipe”, *Lond Edinb Dubl Phil Mag*, Vol. 4 (20), pp. 208–223.

[2] Jokiel, M., Wagner, L.-M., Mansour, M., Kaiser, N. M., Zähringer, K., Janiga, G., Nigam, K. D., Thevenin, D., and Sundmacher, K., 2017, “Measurement and simulation of mass transfer and backmixing behavior in a gas-liquid helically coiled tubular reactor”, *Chem Eng Sci*, Vol. 170, pp. 410–421.

[3] Mansour, M., Liu, Z., Janiga, G., Nigam, K. D., Sundmacher, K., Thévenin, D., and Zähringer, K., 2017, “Numerical study of liquid-liquid mixing in helical pipes”, *Chem Eng Sci*, Vol. 172, pp. 250–261.

[4] Mansour, M., Khot, P., Thévenin, D., Nigam, K. D., and Záhringer, K., 2020, “Optimal Reynolds number for liquid-liquid mixing in helical pipes”, *Chem Eng Sci*, Vol. 214, p. 114522.

[5] Mansour, M., Landage, A., Khot, P., Nigam, K. D., Janiga, G., Thévenin, D., and Záhringer, K., 2020, “Numerical study of gas–liquid two–phase flow regimes for upward flow in a helical pipe”, *Ind Eng Chem Res*, Vol. 59 (9), pp. 3873–3886.

[6] Mansour, M., Thévenin, D., Nigam, K. D. P., and Zähringer, K., 2019, “Generally-valid optimal Reynolds and Dean numbers for efficient liquid-liquid mixing in helical pipes”, *Chem Eng Sci*, Vol. 201, pp. 382–385.

[7] Khot, P., Mansour, M., Thévenin, D., Nigam, K. D. P., and Zähringer, K., 2019, “Improving the mixing characteristics of coiled configurations by early flow inversion”, *Chem Eng Res Des*, Vol. 146, pp. 324–335.

[8] Mansour, M., Zähringer, K., Nigam, K. D., Thévenin, D., and Janiga, G., 2020, “Multi-objective optimization of liquid-liquid mixing in helical pipes using Genetic Algorithms coupled with Computational Fluid Dynamics”, *Chem Eng J*, Vol. 391, p. 123570.

[9] Mansour, M., Thévenin, D., and Zähringer, K., 2020, “Numerical study of flow mixing and heat transfer in helical pipes, coiled flow inverters and a novel coiled configuration”, *Chemical Engineering Science*, Vol. 221, p. 115690.

[10] Ali, N., and Mandal, M. M., 2019, "Immiscible liquid-liquid flow in coiled tube", *International Conference on Sustainable and Innovative Solutions for Current Challenges in Engineering & Technology*, Springer, pp. 307–319.

[11] Gelfgat, A. Y., Yarin, A., and Bar-Yoseph, P., 2003, "Dean vortices-induced enhancement of mass transfer through an interface separating two immiscible liquids", *Phys Fluids*, Vol. 15 (2), pp. 330–347.

[12] Zhang, J., Guo, J., Gong, D.-t., Wang, L.-y., Tang, C., and Zheng, Z.-c., 2006, "An investigation on oil/water separation mechanism inside helical pipes", *J Hydrodyn*, Vol. 18 (1), pp. 336–340.

[13] Zhang, Y., Guo, C., Hou, H., and Xue, G., 2014, "Experimental research and numerical simulation on gas-liquid separation performance at high gas void fraction of helically coiled tube separator", *Int J Chem Eng*, Vol. 2014.

[14] Sharma, M., Ravi, P., Ghosh, S., Das, G., and Das, P., 2011, "Studies on low viscous oil–water flow through return bends", *Exp Therm Fluid Sci*, Vol. 35 (3), pp. 455–469.

[15] Pietrzak, M., 2014, "Flow patterns and volume fractions of phases during liquid–liquid two-phase flow in pipe bends", *Exp Therm Fluid Sci*, Vol. 54, pp. 247–258.

[16] Al-Azzawi, M., Mjalli, F. S., Husain, A., and Al-Dahhan, M., 2021, "A review on the hydrodynamics of the liquid–liquid two-phase flow in the microchannels", *Ind Eng Chem Res*, Vol. 60 (14), pp. 5049–5075.

[17] Weiwei, E., Pope, K., and Duan, X., 2020, "Separation dynamics of immiscible liquids", *SN Appl Sci*, Vol. 2 (12), pp. 1–14.

[18] Hartman, R. L., Sahoo, H. R., Yen, B. C., and Jensen, K. F., 2009, "Distillation in microchemical systems using capillary forces and segmented flow", *Lab Chip*, Vol. 9 (13), pp. 1843–1849.

[19] Culbertson, C. T., Jacobson, S. C., and Ramsey, J. M., 2000, "Microchip devices for high-efficiency separations", *Anal Chem*, Vol. 72 (23), pp. 5814–5819.

[20] Juang, D. S., Berry, S. M., Li, C., Lang, J. M., and Beebe, D. J., 2019, "Centrifugation-assisted immiscible fluid filtration for dual-bioanalyte extraction", *Anal Chem*, Vol. 91 (18), pp. 11848–11855.

[21] von Deylen, J., Köpplin, J., and Thévenin, D., 2022, "Development and Validation of a Design Tool for an Improved Pitot-Tube Jet-Pump Allowing Continuous Fluid-Fluid Separation", *J Fluids Eng*, Vol. 144 (7), 071401.

[22] Steinhoff, J., Charlafti, E., Leleu, D., Reinecke, L., Franken, H., Becker, K., Kalem, M., Sixt, M., Braß, M., Borchardt, D., et al., 2021, "Energy and resource savings through innovative and CFD-based design of liquid/liquid gravity separators", *Chem Ing Tech*.

[23] da Mota, F. R., and Pagano, D. J., 2014, "Simulation and experimental study of phase segregation in helical pipes: A new method for flow conditioning", *Flow Meas Instrum*, Vol. 35, pp. 99–108.

[24] Xu, B., Zhang, X., Zhao, L., Jiang, M., Liu, L., and Xia, H., 2020, "Structure design and preliminary experimental investigation on oil-water separation performance of a novel helix separator", *Sep Sci Technol*, pp. 1–12.

[25] Kováts, P., Martins, F. J., Mansour, M., Thévenin, D., and Zähringer, K., 2020, "Tomographic PIV measurements and RANS simulations of secondary flows inside a horizontally positioned helically coiled tube", *Exp Fluids*, Vol. 61 (5), pp. 1–15.

[26] Kováts, P., Velten, C., Mansour, M., Thévenin, D., and Zähringer, K., 2020, "Mixing characterization in different helically coiled configurations by laser-induced fluorescence", *Exp Fluids*, Vol. 61 (9), pp. 1–17.

[27] Mansour, M., Kasetti, S., Thévenin, D., Nigam, K. D., and Zähringer, K., 2021, "Numerical study of the separation of two immiscible liquids in helical and straight pipes", *Chem Eng Process*, p. 108654.

[28] Mansour, M., Parikh, T., Engel, S., Wunderlich, B., and Thévenin, D., 2020, "Numerical investigations of gas-liquid two-phase flow in a pump inducer", *J Fluids Eng*, Vol. 142 (2), pp. 021302–1–021302–12.

[29] Kopparthy, S., Mansour, M., Janiga, G., and Thévenin, D., 2020, "Numerical investigations of turbulent single-phase and two-phase flows in a diffuser", *Int J Multiph Flow*, Vol. 130, p. 103333.

[30] Parikh, T., Mansour, M., and Thévenin, D., 2020, "Investigations on the effect of tip clearance gap and inducer on the transport of air-water two-phase flow by centrifugal pumps", *Chem Eng Sci*, Vol. 218, p. 115554.

[31] Mansour, M., Parikh, T., and Thévenin, D., 2020, "Influence of blade pitch and number of blades of a pump inducer on single and two-phase flow performance", *ASME Turbo Expo 2020: Turbomachinery Technical Conference and Exposition*, American Society of Mechanical Engineers, p. V009T21A010.

[32] Mansour, M., Khot, P., Kováts, P., Thévenin, D., Zähringer, K., and Janiga, G., 2019, "Impact of computational domain discretization and gradient limiters on CFD results concerning liquid mixing in a helical pipe", *Chem Eng J*, Vol. In Press, (2019), p. 123121.